2013

Numerical Study of Gas-Solid Fluidized Beds: Aanalysis of Pressure Fluctuations for Detection of Disturbed Fluidization

Philipp Wiedemann
Brandenburg University of Technology Cottbus, Germany

Hans Joachim Krautz
Brandenburg University of Technology Cottbus, Germany

NUMERICAL STUDY OF GAS-SOLID FLUIDIZED BEDS: ANALYSIS OF PRESSURE FLUCTUATIONS FOR DETECTION OF DISTURBED FLUIDIZATION

Philipp Wiedemann*, Hans Joachim Krautz
Brandenburg University of Technology Cottbus, Chair of Power Plant Technology
PO Box 101344, 03013 Cottbus, Germany
*Tel.: +49 (0) 355 693692, E-Mail: philipp.wiedemann@tu-cottbus.de

ABSTRACT

Numerical simulations using the Two Fluid Model are performed for gas-solid bubbling fluidized beds. The possibility to detect disturbances in the fluidization process is investigated by common analysis of pressure fluctuations and variation of the computational domain. Additionally the influences of different particle sizes and superficial gas velocities are studied. The results are compared with bubble properties obtained from a digital image analysis technique.

INTRODUCTION

Fluidized beds are widely applied in process engineering due to their high mixing rates and thus excellent heat and mass transfer. For drying of wet granules they often contain heated horizontal tubes to increase the heat transfer. If the entering particles feature high moisture content and tend to agglomeration, sticking or adherence to these internal obstacles could occur. For continuing growth of the agglomerate the fluidization hydrodynamics get disturbed reducing the efficiency of the process. The detection of such disturbances is difficult because there is no possibility for visual observation in most chemical and thermal applications due to the harsh operating conditions of the system. Hence measurement and analysis of pressure fluctuations is a reasonable tool for process monitoring as proposed by van Ommen et al. (1), Sasic et al. (2) and Gallucci et al. (3).
In preparation for experimental investigations this study pursues the objective to distinguish between absence and presence of disturbances in fluidization by common analysis of the pressure signal. Therefor CFD simulations for a pseudo two-dimensional lab-scale fluidized bed of Geldart B particles (glass beads) with immersed horizontal tubes are performed. In general there are two methods for modelling the two-phase flow of gas-solid fluidized beds. By using the Discrete Particle Method (DPM), the equation of motion is solved for each particle. This method offers more accurate results but leads to enormous computational effort concerning the huge amount of particles in the present study. In contrast to the DPM the Two Fluid Model (TFM) bases on the Euler-Euler approach, viz. treating both the gas and the solid phase as continua. Thereby closure models for the description of the solid phase and its interaction with the gas phase are necessary. Previous

studies demonstrated that the TFM is able to predict the hydrodynamics of bubbling fluidized beds satisfactorily (cf. (4-7)) and thus can be used for data generation in this study.

MATHEMATICAL MODELLING

Governing Equations and Closure Models

For modelling the gas-solid flow, the Two Fluid Model is chosen. The conservation equations of mass and momentum are shown in Table 1 for each phase. The volume fractions are related as $\varepsilon_g + \varepsilon_s = 1$. For the description of the solid phase, the Kinetic Theory of Granular Flow is applied. The conservation equation of Granular Temperature is used in algebraic form (see Table 1) as proposed by Syamlal et al. (8). The shear stress tensors are assumed to be Newtonian for both phases. Thereby the bulk viscosity of the gas phase is neglected. The closure models that are used for the solid phase and the drag law are presented in Table 2. Additionally Table 3 shows the physical properties and simulation parameters. The solution is accomplished by the commercial CFD-code ANSYS Fluent 12.1.

Table 1: Governing equations

Conservation of mass

$$\frac{\partial(\varepsilon_g \rho_g)}{\partial t} + \nabla \cdot \left(\varepsilon_g \rho_g \vec{v}_g\right) = 0$$

$$\frac{\partial(\varepsilon_s \rho_s)}{\partial t} + \nabla \cdot \left(\varepsilon_s \rho_s \vec{v}_s\right) = 0$$

Conservation of momentum

$$\frac{\partial(\varepsilon_g \rho_g \vec{v}_g)}{\partial t} + \nabla \cdot \left(\varepsilon_g \rho_g \vec{v}_g \vec{v}_g\right) = \varepsilon_g \nabla \cdot \bar{\bar{\tau}}_g - \varepsilon_g \nabla p + \varepsilon_g \rho_g \vec{g} - \beta\left(\vec{v}_g - \vec{v}_s\right)$$

$$\frac{\partial(\varepsilon_s \rho_s \vec{v}_s)}{\partial t} + \nabla \cdot \left(\varepsilon_s \rho_s \vec{v}_s \vec{v}_s\right) = \varepsilon_s \nabla \cdot \bar{\bar{\tau}}_s - \varepsilon_s \nabla p - \nabla p_s + \varepsilon_s \rho_s \vec{g} + \beta\left(\vec{v}_g - \vec{v}_s\right)$$

Conservation of Granular Temperature

$$0 = \left(-p_s \bar{\bar{I}} - \bar{\bar{\tau}}_s\right) : \nabla \vec{v}_s - \gamma_s$$

Table 2: Closure models

Parameter	Model	Ref.
Solid shear viscosity	Gidaspow	(9)
Solid bulk viscosity	Lun et al.	(10)
Frictional viscosity	Schaeffer	(11)
Frictional pressure	Johnson et al.	(12)
Solid pressure	Lun et al.	(10)
Radial distr. function	Ma, Ahmadi	(13)
Drag Law	Gidaspow	(9)

Table 3: Physical properties and simulation parameters

Parameter	Value	Unit
Solid density	2500	kg/m³
Solid diameter	246, 347, 439	µm
Maximum packing limit	0.65	
Initial solid volume fraction	0.62	
Initial bed height	0.5	m
Superficial gas velocity	0.135 ... 0.5675	m/s
Gas density	1.2	kg/m³
Gas shear viscosity	1.79×10^{-5}	kg/(m s)
Angle of internal friction	28.5	°
Restitution coefficient	0.95	
Frictional packing limit	0.60	

Geometry and Grid

In this paper two different geometries are investigated, cf. Figure 1. The default case is shown in the left part of the figure, where six rows of tubes in a staggered arrangement can be seen. For the simulation of adhering agglomerates an arbitrary cut-off is realized for the disturbed case (right part). In both cases the geometry is 20 mm in depth. The computational mesh consists of 5 mm hexagonal cells which are refined down to 2 mm near the tubes to catch the higher velocity gradients there. The total number of cells is 99104 for the default cases and 79464 for the disturbed ones. The simulations are performed three-dimensionally for correct prediction of dynamic behaviour as suggested by Peirano et al. (7).

Boundary and Initial Conditions, Numerical Setup

The initial bed height is 500 mm at minimum fluidization conditions. At the top a pressure outlet boundary condition is chosen. At the bottom a velocity inlet boundary condition with uniform velocity for the gas phase is applied. For the four walls and the tubes' surfaces a no-slip boundary condition for the gas phase and a partial slip boundary condition (14) with a specularity coefficient of 0.5 for the solid phase are assumed. PC-SIMPLE is selected for pressure-velocity coupling. The discretization schemes are 2nd order implicit for time, 2nd order upwind for momentum and QUICK for continuity. $5x10^{-5}$ s are chosen for time step size.

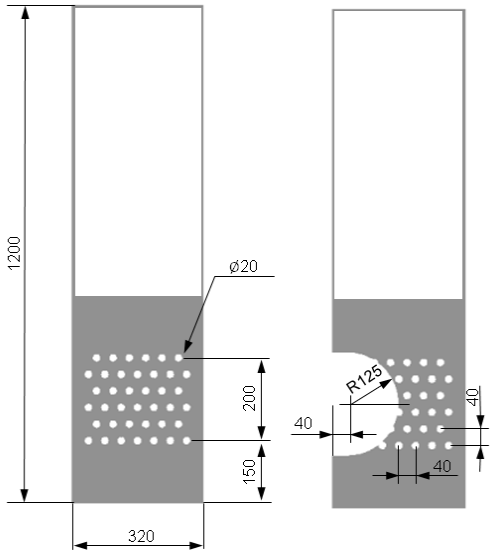

Figure 1: Geometries for absence (left) and presence (right) of disturbance with staggered tube arrangement (in mm)

The mathematical model in combination with the mentioned grid size was validated for correct prediction of time averaged behaviour by Asegehegn et al. (4, 5) using a digital image analysis technique (cf. (15)) among others.

Extraction of Pressure Signal

The pressure is extracted on the right boundary wall of the geometry at a distance of 200 mm above the inlet. The position is chosen according to van Ommen et al. (16). 20 s of flow time are simulated where the first 5 s are neglected to avoid start-up effects. So the pressure data is sampled for a flow time of 15 s with a frequency of 1 kHz which allows a resolution up to 500 Hz according to the Shannon-Nyquist-theorem.

RESULTS AND DISCUSSION

Validation of the Model for Dynamic Behaviour

The validity of the described set up for dynamic behaviour is verified by the evaluation of dynamic characteristics obtained from the pressure signal. First a comparison of the most dominant frequencies with the theories of Baskakov et al. (17) and Roy et al. (18) is drawn. When doing so, the frequency range below 10 Hz, representing larger bubble structures, is observed. Therefor the extracted pressure data is transformed into the frequency domain and analyzed appropriately.

The model of Baskakov et al. (17) assumes a fluidized bed where only a single bubble at a time erupts at the bed surface. They suggested that this phenomenon is

similar to the oscillation of an incompressible liquid in a U-shaped tube where its natural frequency can be described by the following equation.

$$f_d = \frac{1}{\pi}\sqrt{\frac{g}{H_{mf}}}$$

In contrast, the model of Roy et al. (18) is based upon multiple bubble eruptions at the bed surface. The dominant frequency is given by:

$$f_d = \frac{1}{4H_{mf}}\sqrt{\frac{p}{\rho_p(1-\varepsilon_{g,mb})\varepsilon_{g,mb}}}$$

The results of the simulations tend to obey the theory of Baskakov et al. (17) as can be seen from Figure 2. This leads to the assumption of single bubble eruptions at the bed surface, despite the existence of immersed tubes provoking splitting of bubbles. However, it has been shown by Asegehegn et al. (15) that the influence of immersed horizontal tubes on the bubble properties is stringently restricted to their location in the bed (i.e. 150 to 350 mm of the running bed height in this work). Viz. the space above the tube bank is sufficient for the coalescence of numerous small bubbles to a single larger one erupting at the bed surface. In case of the simulated disturbance (cf. Figure 1, right part) the bubbles are forced to coalesce anyway due to the reduction of the flow cross-section.

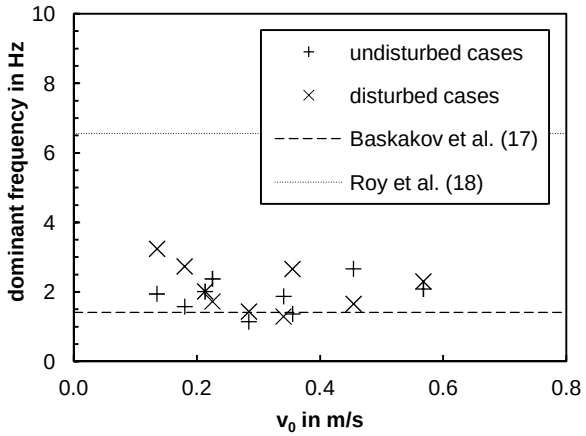

Figure 2: Dominant frequencies of the simulated pressure fluctuations

Furthermore, the slopes of the power spectra of the pressure fluctuations are investigated. It is shown in the literature (1) that the region after about 10 Hz represents finer structures of the process and the decay of the power spectral density can be described via a power-law. In doing so, a stochastic character is imputed to the system. Several authors (van Ommen et al. (1), Sasic et al. (2), etc.) investigated this phenomenon in detail and found the value of the

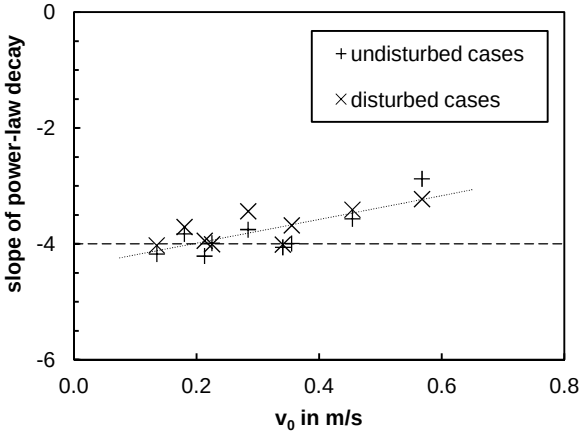

Figure 3: Slopes of power-law decay of the simulated pressure fluctuations

power-law slope to be in the order of -4. Figure 3 compares the simulated results with the theoretical prediction. Besides their quantitative agreement, a slight growth with increasing superficial velocity can be recognized. This seems to be compliant with results presented by van Wachem et al. (6) where the slope of the power-law decay is about -3.6 for superficial velocities above 0.5 m/s.

In summary the results for dominant frequencies and power-law slopes are in good agreement with the presented theories. Consequently the Two Fluid Model used is not only able to predict the time averaged behaviour of fluidized beds but also the dynamics satisfactorily.

Detection of Disturbed Fluidization

The disturbance of fluidization by adhering agglomerates is investigated for particle diameters of 246 µm, 347 µm, 439 µm and superficial velocities 1.5, 2.0, 2.5 times the minimum fluidization velocity respectively. As described in the introduction, adhering agglomerates influence the fluidization hydrodynamics and reduce the mixing of particles. This effect can be confirmed by Figure 4, where the time averaged mass flux vectors of the solid phase are compared exemplarily for both the undisturbed and the disturbed case. On the left side the typical axis-symmetric flow pattern with nearly ideal recirculation of the particles to the gas inlet can be observed. This is not the case for the right side. The particles seem to follow a diagonal jet which leads to the formation of an upper left and a lower right circulation. In addition, the mass flux is near zero straight above the adherence due to the missing fluidization. Consequently these particles are excepted from mixing and have no chance to take advantage of the high heat and mass transfer rates in the tube bank region favouring the problem of agglomeration.

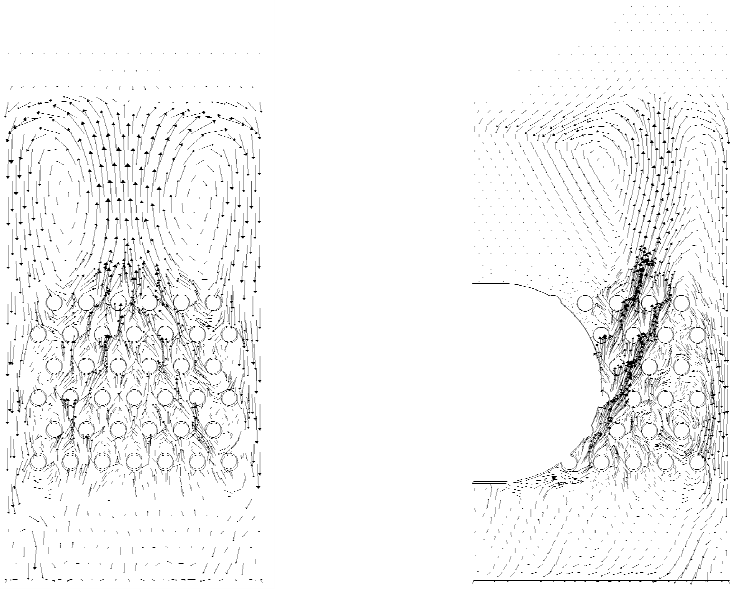

Figure 4: Comparison of undisturbed (left) and disturbed (right) fluidization by time averaged mass flux vectors of the solid phase (246 µm, 2.0 v_{mf}; not to scale)

For detection of such phenomena the analysis of the pressure signal in the time domain is performed at first. The standard deviation (i.e. the second order statistical moment) of the time series can be interpreted as a mean amplitude of the pressure fluctuations as mentioned in the literature (1, 2). It seems reasonable to plot their ratios of disturbed to undisturbed cases (see Figure 5), instead of absolute values. One can see that the ratios are much greater than unity for all cases denoting eruptions of larger bubbles at the bed surface due to their forced coalesce by reduction of the flow cross-section. Additionally two other phenomena can be observed from Figure 5. On the one hand the ratio of the mean amplitudes decreases with increasing superficial velocity, because the contribution to the regime transition to slugging flow by disturbance gets smaller at higher velocities. Viz. the effect of the adherence is less important for higher velocities. On the other hand the particle diameter influences the bubble size anyway as shown by Asegehegn et al. (15). So the increase of bubble size by presence of a disturbance is smaller for particles with larger diameter.

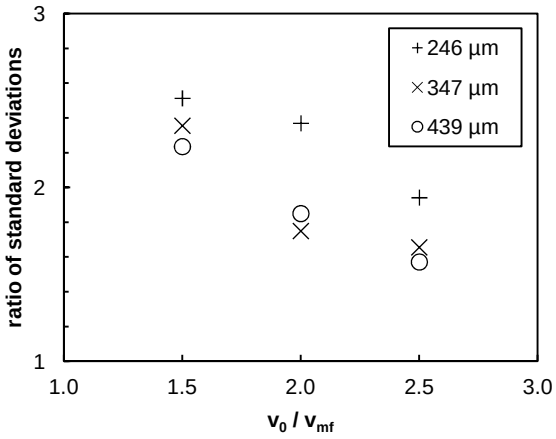

Figure 5: Ratio of standard deviations of disturbed to undisturbed fluidization in dependence of superficial velocity and particle diameter

Referring to (1) the picture for the identification of a regime change from bubbling to slugging flow gets clearer when taking pressure drop data into account. In case of disturbed fluidization the averaged bed pressure drop is reduced by one third up to the half concerning all simulated cases. However, when considering the reduction of the loaded mass in the simulation, the effective decline of pressure drop is merely about 15 to 30 percent. Anyway, the effect results from the particles that are placed in the lee zone above the adherence. They are resting on the latter one and are not fluidized as already shown by Figure 4 (right part).

Furthermore the frequency domains of the simulated pressure fluctuations are analyzed. As already shown in Figure 2, the dominant frequencies denote single bubble eruptions at the bed surface for all cases, but no clear tendency can be detected for the regime change. The continuance of the stochastic character of the system is verified by the ratio of the power-law slopes remaining close to unity (cf. Figure 6).

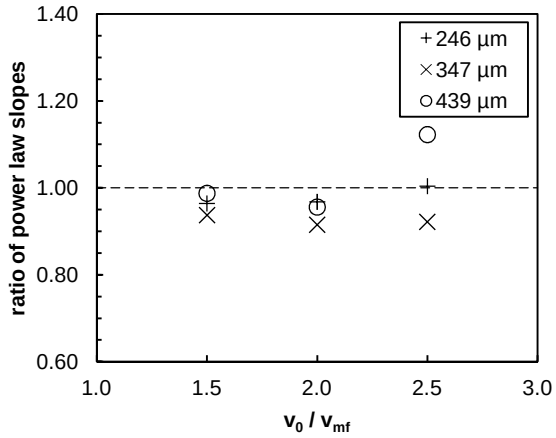

Figure 6: Ratio of power-law slopes of disturbed to undisturbed fluidization in dependence of superficial velocity and particle diameter

Comparison with Digital Image Analysis

The effect of decreasing contribution to regime transition at higher velocities in case of disturbance, as described above, is acknowledged by usage of the digital image analysis technique presented by Asegehegn et al. (15). Figure 7 indicates the distribution of the ratio of time averaged bubble diameters along the bed height above the tube bank exemplarily for the particle size of 347 µm. In agreement with Figure 5 the influence of the adherence is most dominant for the smallest superficial velocity and reduces in an analogue relationship for further increase. Additionally it can be seen from the values being close to unity (in Figure 7) that analyzing the pressure signal allows detection of disturbances whereas image analysis does not for all investigated velocities.

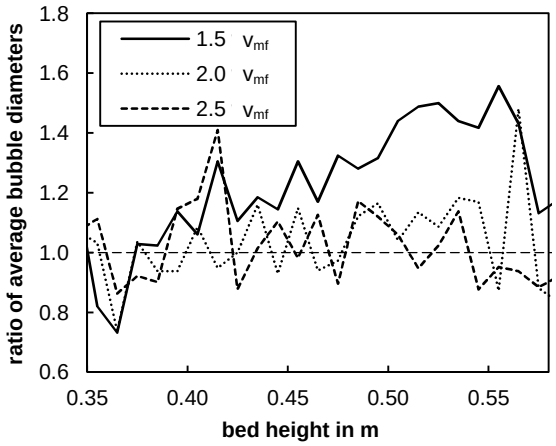

Figure 7: Ratio of time averaged bubble diameters of disturbed to undisturbed fluidization vs. bed height (347 µm)

Anymore, the image analysis offers the expanded bed height averaged for the 15 s of flow time. If again the ratios of undisturbed to disturbed cases are examined for this parameter, the values are slightly below unity always. The not insignificant amount non-fluidized particles straight above the adherence are suggested to be the reason for it.

CONCLUSION

Numerical simulations using the Two Fluid Model were performed for two versions of a lab-scale fluidized bed representing absence and presence of adherences. In order to distinguish these, pressure fluctuations were analyzed for different particle sizes and superficial velocities. The main influences were carried out and confirmed by using a digital image analysis technique. For the purpose of applying the analysis of pressure fluctuations for detection of disturbed fluidization practically, further research needs to be done. Thereby different sizes, shapes and locations of the disturbance should be investigated.

ACKNOWLEDGEMENT

The authors gratefully acknowledge the funding of this research project by the German Federal Ministry of Economics and Technology within the “COORETEC” initiative as well as the industrial cooperation partners.

NOTATION

Symbols

f	frequency, Hz
g	gravitational acceleration, m/s²
H	bed height, m
I	unit tensor
p	pressure, Pa
t	time, s
v	velocity, m/s
β	interphase drag coefficient, kg/(m³s)
γ	dissipation of fluctuating energy, kg/(m³s)
ε	volume fraction
ρ	density, kg/m³
τ	shear stress tensor, N/m²

Subscripts

0	for superficial velocity
d	dominant
g	gas phase
mb	minimum bubbling
mf	minimum fluidization
p	particle
s	solid phase

REFERENCES

1. J.R. van Ommen, S. Sasic, J. van der Schaaf, S. Gheorghiu, F. Johnsson, M.-O. Coppens: Int. J. Multiphase Flow 37 (2011) 403-428
2. S. Sasic, B. Leckner, F. Johnsson: Progr. Energ. Combust. Sci. 33 (2007) 453-496
3. K. Gallucci, N. Jand, P.U. Foscolo, M. Santini: Chem. Eng. J. 87 (2002) 61-71
4. T.W. Asegehegn: Investigation of Bubble Hydrodynamics in Gas-Solid Fluidized Beds Containing Immersed Horizontal Tube Banks for Lignite Drying Application. Dissertation. Brandenburg University of Technology Cottbus. 2012
5. T.W. Asegehegn, M. Schreiber, H.J. Krautz: Powder Technol. 219 (2012) 9-19
6. B.G.M. van Wachem, J.C. Schouten, R. Krishna, C.M. van den Bleek: Chem. Eng. Sci. 54 (1999) 2141-2149
7. E. Peirano, V. Delloume, B. Leckner: Chem. Eng. Sci. 56 (2001) 4787-4799
8. M. Syamlal, W. Rogers, T.J. O'Brien: MFIX Documentation Theory Guide. U.S. Dept. of Energy. 1993. DOE/METC-95/1004 (DE9400087)
9. D. Gidaspow: Multiphase Flow and Fluidization: Continuum and Kinetic Theory Descriptions. 1994. Academic Press, Boston
10. C.K.K. Lun, S.B. Savage, D.J. Jeffrey, N. Chepurniy: J. Fluid Mech. 140 (1984) 223-256
11. D.G. Schaeffer: J. Diff. Eq. 66 (1987) 19-50
12. P.C. Johnson, P. Nott, R. Jackson: J. Fluid Mech. 210 (1990) 501-535
13. D. Ma, G. Ahmadi: Int. J. Multiphase Flow 16 (1990) 323-351
14. P.C. Johnson, R. Jackson: J. Fluid Mech. 176 (1987) 67-93
15. T.W. Asegehegn, M. Schreiber, H.J. Krautz: Powder Technol. 210 (2011) 248-260
16. J.R. van Ommen, J. van der Schaaf, J.C. Schouten, B.G.M. van Wachem, M.-O. Coppens, C.M. van den Bleek: Powder Technol. 139 (2004) 264-276
17. A.P. Baskakov, V.G. Tuponogov, N.F. Filippovsky: Powder Technol. 45 (1986) 113-117
18. R. Roy, J.F. Davidson, V.G. Tuponogov: Chem. Eng. Sci. 45 (1990) 3233-3245